Computers and Concrete, *Vol. 15, No. 5 (2015) 735-758*
DOI: http://dx.doi.org/10.12989/cac.2015.15.5.735

Modeling of unilateral effect in brittle materials by a mesoscopic scale approach

José J.C. Pituba*[1] and Eduardo A. Souza Neto[2a]

[1]Department of Civil Engineering, Federal University of Goiás, Campus Catalão
Av Dr Lamartine Pinto de Avelar, 1120, Setor Universitário, Catalão, Goiás, Brazil, 75740-020
[2]Civil and Computational Engineering Centre, School of Engineering, Swansea University
Singleton Park, Swansea SA2 8PP, United Kingdom

(Received April 25, 2013, Revised January 23, 2015, Accepted January 24, 2015)

Abstract. This work deals with unilateral effect of quasi-brittle materials, such as concrete. For this propose, a two-dimensional meso-scale model is presented. The material is considered as a three-phase material consisting of interface zone, matrix and inclusions – each constituent modeled by an appropriate constitutive model. The Representative Volume Element (RVE) consists of inclusions idealized as circular shapes randomly placed into the specimen. The interface zone is modeled by means of cohesive contact finite elements developed here in order to capture the effects of phase debonding and interface crack closure/opening. As an initial approximation, the inclusion is modeled as linear elastic as well as the matrix. Our main goal here is to show a computational homogenization-based approach as an alternative to complex macroscopic constitutive models for the mechanical behavior of the quasi-brittle materials using a finite element procedure within a purely kinematical multi-scale framework. A set of numerical examples, involving the microcracking processes, is provided. It illustrates the performance of the proposed model. In summary, the proposed homogenization-based model is found to be a suitable tool for the identification of macroscopic mechanical behavior of quasi-brittle materials dealing with unilateral effect.

Keywords: multi-scale analysis; constitutive model; quasi-brittle materials; unilateral effect; cohesive contact finite element

1. Introduction

This works deals with numerical applications of a computational homogenization-based approach proposed to model the mechanical behavior of quasi-brittle materials subject to reversal loading. The goal of this work is to contribute to modeling of bimodular materials that present recovery of elastic properties due to crack closure. The proposed approach can be seen as an alternative to complex macroscopic constitutive models for the mechanical behavior of the quasi-brittle materials using a finite element procedure within a purely kinematical multi-scale framework (Peric *et al.* 2011, Giusti *et al.* 2009).

Many damage models have been proposed using phenomenological or micromechanical

∗Corresponding author, Professor, E-mail: julio_pituba@ufg.br
[a] Professor, E-mail: E.deSouzaNeto@swansea.ac.uk

http://www.techno-press.org/?journal=cac&subpage=8 ISSN: 1598-8198 (Print), 1598-818X (Online)

approaches (Pituba and Fernandes 2011, Brancherie and Ibrahimbegovic 2009, Zhu *et al.* 2008 and others). The unilateral effects and crack interaction effects are not properly described in many phenomenological damage models, (Zhu *et al.* 2009). Therefore, some features of quasi-brittle materials still need to be investigated, such as, the unilateral effect. Complex formulations, excessive number of parameters to identify and, even, in some cases, parameters without physical meaning, are problems to overcome using phenomenological constitutive models.

In the other hand, in the last decade, many works deal with the prediction of mechanical behavior of materials using information about two or more physical scales (Miehe *et al.* 1999, Michel *et al.* 1999, Terada *et al.* 2003, Giusti *et al.* 2009, Gal and Kryvoruk 2011). It can be noted that some works dealing with modeling of mechanical behavior of concrete have the advantage to capture some important features. However, complex formulations are used in order to model the materials involved (Unger *et al.* 2011a, Unger *et al.* 2011b, Verhoosel *et al.* 2010, He *et al.* 2011). Initially, this work intends to simulate the mechanical behavior of the concrete using constitutive models simplest as possible. Potentialities and limitations about the use of the proposed model are discussed. Accordingly with, the material is considered as a three-phase material consisting of interface zone, matrix (cement paste) and inclusions (aggregates) – each constituent modeled by an appropriate constitutive model. The Representative Volume Element (RVE) consists of aggregates idealized as circular shapes randomly placed into the concrete specimen. The interface zone is modeled by cohesive contact finite elements developed in this work in order to capture the effects of phase debonding and interface crack closure/opening. As an initial approximation, the aggregate is modeled as linear elastic as well as the cement paste. Then, we are trying to model a complex macroscopic behavior using simplest as possible as constitutive models at mesoscopic scale taking into account the geometry of the material phases and the dissipative phenomena in the interfacial transition zone (ITZ).

Others works have attempted to model the mechanical behavior of concrete by means cohesive fracture model (Ortiz and Pandolfi 1999, Carol *et al.* 2001, Cirak *et al.* 2005) using some interface finite elements, but in those works the aim have been to model the crack opening. In this work, the proposed approach intends to deal with unilateral effect presented in some heterogeneous materials, like concrete. Therefore, a cohesive contact finite element has been developed.

This work is divided into six sections. In section 2, the kinematical multi-scale framework is described. In section 3, the constitutive models are briefly presented. After that, the development of the cohesive contact finite element is described in section 4. The section 5 shows some numerical results related to microcraking process on the RVE, mainly about unilateral effect simulations. The paper ends in section 6 where some concluding remarks, limitations and possible extensions of the model are discussed.

2. Multi-scale constitutive modeling

This section intends to review the multi-scale constitutive framework (Giusti *et al.* 2009, Peric *et al.* 2011) used here to estimate the macroscopic elasticity tensor from the knowledge of the underlying material microstructure.

Following (Somer *et al.* 2009), the class of multi-scale solid mechanics problems with which the present paper is concerned is characterized by:

(1) A conventional equilibrium boundary value problem at the so called macroscopic scale, where

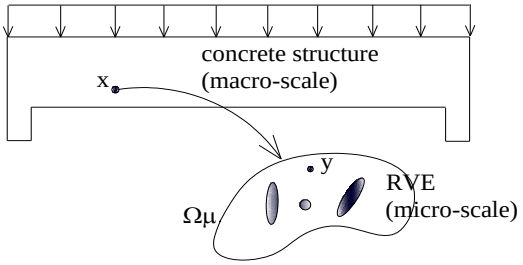

Fig. 1 Macroscopic continuum represented by a concrete beam and the Representative Volume Element (RVE) of the heterogeneous material

(2) The constitutive response at each point of the macroscopic continuum is defined in a non-conventional way by homogenizing the response of a representative volume element (RVE) that models the material micro structure at that point (see Fig. 1). The RVE itself is modeled as a conventional (generally dissipative) continuum and the macroscopic stress and strain tensor are volume averages of their so-called microscopic counterparts over the RVE.

The starting point of the kinematically-based family of multi-scale constitutive theories upon which the present paper relies is the assumption that any material point x of the (macroscopic) continuum is associated to a local Representative Volume Element (RVE). At any instant t, the strain tensor at an arbitrary point x of the macro-continuum is assumed to be the volume average of the microscopic strain tensor field, $\boldsymbol{\varepsilon}_\mu$, defined over the RVE domain Ω_μ

$$\varepsilon_\mu(t)=\frac{1}{V_\mu}\int_{\Omega_\mu}\varepsilon_\mu(y,t)dV \tag{1}$$

where V_μ is the volume of the RVE and $\boldsymbol{\varepsilon}_\mu=\nabla^s\mathbf{u}_\mu$, the symmetric gradient of the microscopic displacement field $\mathbf{u}_\mu$ of the RVE.

In Peric *et al.* (2011) is showed that the averaging relation Eq. (1) is equivalent to the following constraint on the displacement field of the RVE

$$\int_{\partial\Omega_\mu} u_\mu \otimes_S n dA = V_\mu \varepsilon \tag{2}$$

where $\mathbf{n}$ denotes the outward unit normal field on Ω_μ.

This constraint requires the set χ_μ of kinematically admissible RVE displacement fields to be a subset of the minimally constrained set of kinematically admissible microscopic displacements χ_μ^*:

$$\chi_\mu \subset \chi_\mu^* \equiv \left\{ v, \textit{sufficienly regular} / \int_{\partial\Omega_\mu} v \otimes n dA = V_\mu \varepsilon \right\} \tag{3}$$

with sufficiently regular meaning that the relevant functions have the sufficient degree of regularity so that all operations in which they are involved make sense. By splitting $\mathbf{u}_\mu$ into a sum

$$u_\mu(y,t)=\varepsilon(t)y+\tilde{u}_\mu(y,t) \tag{4}$$

of a homogeneous strain displacement, $\boldsymbol{\varepsilon}$(t) y, and a displacement fluctuation field, $\tilde{u}_\mu$. Following the split Eq. (4), the microscopic strain inserted in Eq. (1) can be expressed as the sum

$$\varepsilon_\mu(y,t) = \varepsilon(t) + \nabla^S \tilde{u}_\mu(y,t) \tag{5}$$

of a homogeneous strain field (coinciding with the macroscopic, average strain) and a field $\nabla^s \mathbf{u}_\mu$ that represents a fluctuation about the average.

Similarly to the macroscopic strain definition, the macroscopic stress tensor, $\boldsymbol{\sigma}$, is defined as the volume average of the microscopic stress field, $\boldsymbol{\sigma}_\mu$, over the RVE

$$\sigma_\mu(t) = \frac{1}{V_\mu} \int_{\Omega_\mu} \sigma_\mu(y,t) dV \tag{6}$$

On the other hand, the Hill-Mandel Principle of Macro-Homogeneity for any kinematically admissible motion of the RVE can be expressed by

$$\sigma : \dot{\varepsilon} \equiv \frac{1}{V_\mu} \int_{\Omega_\mu} \sigma_\mu : \dot{\varepsilon}_\mu dV \tag{7}$$

It must hold for any kinematically admissible microscopic strain rate field, $\dot{\varepsilon}_\mu$. Therefore, the variational equilibrium statement – the virtual work equation – for the RVE is given by

$$\int_{\Omega_\mu} \sigma_\mu : \nabla^S \eta dV = 0 \qquad \forall \eta \in \tilde{\chi}_\mu \tag{8}$$

where $\tilde{\chi}_\mu$ is the space of kinematically admissible displacement fluctuations of the RVE. Further, it is assumed that at any time t the stress at each point y of the RVE is delivered by a generic constitutive functional G_y of the strain history $\varepsilon_\mu^t(y)$ at that point up to time t. This constitutive assumption, together with the equilibrium equation, Eq. (8), leads to the definition of the RVE equilibrium problem which consists in finding, for a given macroscopic strain $\boldsymbol{\varepsilon}$ (a function of time), a displacement fluctuation function $\tilde{u}_\mu \in \tilde{\chi}_\mu$ such that

$$\int_{\Omega_\mu^S} G_y \left\{ \left[\varepsilon(t) + \nabla^S \tilde{u}_\mu(y,t) \right]^T \right\} : \nabla^S \eta dV = 0 \qquad \forall \eta \in \tilde{\chi}_\mu \tag{9}$$

The general multi-scale constitutive model in the present context is defined as follows. For a given macroscopic strain history, we must firstly solve the RVE equilibrium problem defined by Eq. (9). With the solution $\tilde{u}_\mu$ at hand, the macroscopic stress tensor is determined according to the averaging relation Eq. (6). The characterization of a multi-scale model of the present type is completed with the choice of a suitable space of kinematically admissible displacement fluctuations, $\tilde{\chi}_\mu \subset \tilde{\chi}_\mu^*$. In general, different choices lead to different macroscopic response functional, Giusti *et al.* (2009). In this work, the periodic and linear boundary fluctuations will be considered in the analysis addressed in Section 5.

The periodic boundary fluctuations are typically associated with the description of media with periodic microstructure. The macrostructure in this case is generated by the periodic repetition of

the RVE. Therefore, considering the description on two-dimensional problems, each pair i of sides consists of equally sized subsets Γ_i^+ and Γ_i^- of $\partial\Omega_\mu$, with respective unit normals n_i^+ and n_i^-, such that $n_i^- = -n_i^+$.

The key kinematical constraint for this class of models is that the displacement fluctuation must be periodic on the boundary of the RVE. That is, for each pair $\{y^+, y^-\}$ of boundary material points we have

$$\tilde{u}_\mu\left(y^+,t\right)=\tilde{u}_\mu\left(y^-,t\right) \tag{10}$$

Accordingly, the space $\tilde{\tilde{\chi}}_\mu$ is defined as

$$\tilde{\tilde{\chi}}_\mu=\tilde{\tilde{\chi}}_{per}\equiv\left\{\tilde{u}_\mu, sufficientlyregular/\tilde{u}_\mu\left(y^+,t\right)=\tilde{u}_\mu\left(y^-,t\right)\forall pair\left\{y^+,y^-\right\}\right\} \tag{11}$$

On the other hand, the linear boundary displacements model is characterized by zero boundary fluctuations. Therefore, the condition below is valid

$$\tilde{\tilde{\chi}}_\mu=\tilde{\tilde{\chi}}_{lin}\equiv\left\{\tilde{u}_\mu, sufficientlyregular/\tilde{u}_\mu(y)=0\forall y\in\partial\Omega_\mu\right\} \tag{12}$$

The displacements of the boundary are fully prescribed as

$$u_\mu(y)=\varepsilon y\forall y\in\partial\Omega_\mu \tag{13}$$

2.1 Numerical approximation

In this work, it is assumed that the constitutive behavior at the RVE level is described by means conventional constitutive theories, such as: cohesive fracture and contact models. The stress tensor is obtained by solving the boundary value problem for a given strain tensor history. Taking into account a set α_n of internal variables related to fracture and contact phenomena addressed here at time t^n, the stress σ_μ^{n+1} is a function of ε_μ^{n+1} at t^{n+1}. The solution to the time-discrete version of the RVE equilibrium problem is given by (Peric *et al.* 2011)

$$\int_{\Omega_\mu^S}\hat{\sigma}_y\left(\varepsilon^{n+1}+\nabla^S\tilde{u}_\mu^{n+1};\alpha_n\right):\nabla^S\eta dV=0,\forall\,\eta\in V_\mu \tag{14}$$

In the general case, the homogenized incremental constitutive function for the stress is defined implicitly through the incremental microscopic equilibrium Eq. (14). The stress σ_μ^{n+1} is obtained by firstly solving Eq. (14) and then, with $\tilde{u}_\mu^{n+1}$ at hand, computing

$$\sigma_{n+1}=\frac{1}{V_\mu}\int_{\Omega_\mu^S}\hat{\sigma}_\mu\left(\varepsilon^{n+1}+\nabla^S\tilde{u}_\mu^{n+1},\Delta t;\alpha_n\right)dV \tag{15}$$

Therefore, the incremental macroscopic stress constitutive function is defined as

$$\hat{\sigma}^{\hom}\left(\varepsilon^{n+1},\Delta t;\alpha_n\right)\equiv\frac{1}{V_\mu}\int_{\Omega_\mu^S}\hat{\sigma}_\mu\left(\varepsilon^{n+1}+\nabla^S\tilde{u}_\mu^{n+1},\Delta t;\alpha_n\right)dV \tag{16}$$

where $\tilde{u}_{\mu}^{n+1}$ is itself a function solely of ε_{μ}^{n+1} (for a given Δt and α_n) defined as the solution of Eq. (14).

Considering a perturbed macroscopic strain that there is a generic incremental strain tensor $\Delta\boldsymbol{\varepsilon}$, the tangential relationship between the macroscopic stress and macroscopic strain tensor at t^{n+1} is expressed by a fourth order tensor D^{hom} consistently with the homogenized incremental constitutive function Eq. (16). That is, for any macroscopic strain direction $\Delta\boldsymbol{\varepsilon}$, we have

$$\hat{\sigma}^{\hom}\left(\varepsilon_{\in},\Delta t;\alpha_n\right)=\hat{\sigma}^{\hom}\left(\varepsilon^{n+1},\Delta t;\alpha_n\right)+\in D^{\hom}:\Delta\varepsilon+o(\varepsilon) \tag{17}$$

where $D^{\hom}:\Delta\varepsilon$ is the directional derivative of the incremental constitutive function $\hat{\sigma}^{\hom}$ in the direction $:\Delta\varepsilon$ and $\in$ is a scalar that contributes with the perturbed macroscopic strain.

Finally, it can be shown in Peric *et al.* (2011) that the following compact canonical formula for the general homogenized incremental constitutive tangent operator can be obtained

$$D^{\hom}+D^{Taylor}+\tilde{D} \tag{18}$$

where $\tilde{D}$ depends on the choice of the kinematical constraints and D^{Taylor} is the volume average of the microscopic incremental constitutive tangent tensor.

3. A mesosocopic mechanical model for concrete

3.1 Finite element modeling

The employed procedure is such that a two-dimensional representation of the concrete is obtained through a slice as input to a mesh generation code that produces a mesh which will be used for two-dimensional mechanical analyses, see Fig. 2. Cohesive fracture finite elements are used to simulate the ITZ whereas triangular finite elements are employed to simulate the aggregates and cement matrix zones. The aggregates are idealized as circular or ellipsoidal shape with various dimensions. They are randomly distributed on RVE. The layout of cement matrix depends on the spatial distribution of aggregate particles.

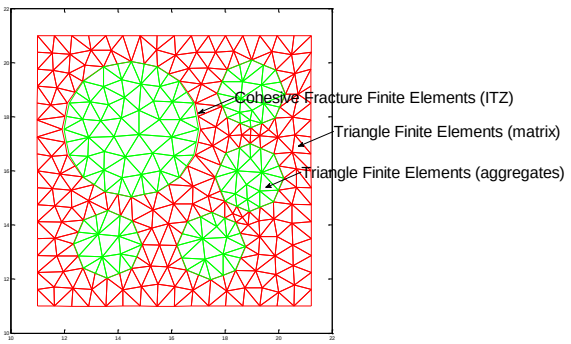

Fig. 2 Finite element model adopted in this work

3.2 Constitutive models

In order to model the fracture processes in materials, cohesive fracture and contact models are adopted in this work. The cohesive fracture model has been originally proposed to simulate opening cracks in solids subject to impact loading (Ortiz and Pandolfi 1999). In general way, the cohesive fracture models were developed to represent the behavior of cracks that have a region capable to transmit efforts between their surfaces, what gradually decreases until there was no such transmission between the surfaces.

On the other hand, when the solid is submitted to loading/unloading, including reversal loading, the crack, previously opened, starts to close. This process leads to stiffness recovery or partial recovery of the material. In heterogeneous materials, like concrete, the friction between the crack surfaces does not allow the complete closure. This phenomenon is a concrete characteristic and it is called unilateral effect, Pituba and Fernandes (2011). Therefore, in order to model the recovery or partial recovery of the elastic moduli, a strategy based on penalty factor is adopted. This strategy has been used because there is an advantage: there are no additional variables in the equations system. Contact Mechanics appeared to avoid the problem created when two bodies or surfaces of a crack are in contact without penetration between the surfaces of bodies or cracks in the numerical model in order to attend the physical model, where the numerical model incorporates a new condition, called impenetrability. Some works which deal with contact problems can be mentioned, for example, Wriggers and Reinelt (2009), Xiaoyu *et al.* (2006) and Wriggers (2006), among others. It can be noted that upon closure, the cohesive surfaces are subject to the contact unilateral constraint, including friction. However, this work does not intend to model the frictional sliding phenomenon in partially closed cracks. This feature can be studied in future works.

The cohesive fracture model proposed by Ortiz and Pandolfi (1999) has been implemented in the finite element code on basis of multi-scale approach described in Section 2. This model is used in order to simulate the opening crack processes on RVE observed in meso-scale throughout loading processes, mainly in the ITZ. Also, this model allows simulating the closing crack processes when the unloading processes take place. Nevertheless, a contact model acts when the crack is completely closed and there is a reversal loading. These both situations are incorporated in the finite element developed in this work and described in Section 4.

A general description about the finite-deformation irreversible cohesive laws is presented in Ortiz and Pandolfi (1999). Some simplified hypotheses are assumed, such as: the behavior of cohesive surfaces is local, the cohesive response is independent of the stretching and shearing of the cohesive surface, the cohesive surface is isotropic, i.e., the resistance to sliding is independent of the direction of sliding. However, these adopted hypotheses lead to good results for the aims of this work.

Therefore, it is assumed here that the cohesive surface is isotropic. This requires that the cohesive free energy ϕ is given by

$$\phi = \phi(\delta_n, \delta_s, q) \tag{19}$$

where $\boldsymbol{\delta_s}$ and $\boldsymbol{\delta_n}$ are the sliding and normal opening displacements, respectively. Also, $\boldsymbol{q}$ is a variable that contains internal variables which describe the inelastic processes attendant to decohesion. Moreover, it is possible to assume that the sliding opening displacement is given by a scalar value independent of direction on crack surface ($\delta_s = |\boldsymbol{\delta_s}|$).

For the formulation of mixed-mode cohesive laws, there is an introduction of an effective opening displacement

$$\delta = \sqrt{\beta^2 \delta_S^2 + \delta_n^2} \tag{20}$$

The parameter β assigns different weights to the sliding and normal opening displacements. Assuming that free energy potential ϕ depends on $\boldsymbol{\delta}$, the cohesive law is written as

$$\boldsymbol{t} = \frac{t}{\delta}(\beta^2 \boldsymbol{\delta_S} + \delta_n \boldsymbol{n}) \tag{21}$$

where $\boldsymbol{n}$ is the normal vector to the crack, $\boldsymbol{\delta_s}$ is the sliding opening displacement vector located on the crack surface, $\boldsymbol{t}$ is the cohesive traction vector over the crack and t is a scalar effective traction given by

$$t = \sqrt{\beta^{-2}|t_S|^2 + t_n^2} \tag{22}$$

This relation shows that β defines the ratio between the shear and the normal critical tractions.

It bears emphasis that, upon closure, the cohesive surfaces are subject to the contact unilateral constraint, including friction. It is regarded that contact and friction are independent phenomena to be modeled outside the cohesive law, Ortiz and Pandolfi (1999).

In this work we have used the following relations to loading Eq. (23) and unloading to the origin Eq. (24)

$$t = e\sigma_c \frac{\delta}{\delta_c} e^{-\delta/\delta_c} \quad if \quad \delta = \delta_{max}, \; and \; \dot{\delta} \geq 0 \tag{23}$$

$$t = \frac{t_{max}}{\delta_{max}} \delta \quad if \quad \delta < \delta_{max}, \; or \; \dot{\delta} < 0 \tag{24}$$

where e is the e-number, σ_c is the maximum cohesive normal traction and δ_c is a characteristic opening displacement.

For the present model, the kinetic relations reduce to

$$\delta_{max} = \begin{cases} \dot{\delta} & if \quad \delta = \delta_{max} \quad and \quad \dot{\delta} \geq 0 \\ 0 & otherwise \end{cases} \tag{25}$$

On the other hand, if the crack is closed, a numerical strategy based on Contact Mechanics is assumed. A penalty factor (λ_p) is adopted in order to avoid a possible penetration between the crack surfaces. This penalty factor is a scalar value parameter. In practice use, high values for the penalty factor are adopted in order to obtain a sufficiently accurate approximation.

In general way, this strategy intends to create stiffness in the node-pairs at the cohesive contact finite element in order to not allow the penetration of the crack surfaces. For detection of the contact phenomenon, this work adopts the concept of the gap between the Gauss points of the cohesive contact finite element described in section 4.

4. Cohesive contact finite element

The phenomena investigated in this work involve a transition from continuum to discrete discontinuity using cohesive fracture models. This kind of problem can be computationally simulated either by enrichment functions or inter-element techniques, Paulino *et al.* (2008).

In this work, it is used the second mentioned technique, where cohesive contact finite element, developed in this section, are inserted between triangular finite elements.

Accordingly with Paulino *et al.* (2008), we are using intrinsic cohesive elements, i.e., the cohesive elements are inserted a priori on the ITZ. This method is easier to develop a mesh generation code because all cohesive contact elements are embedded in the discretized structure prior to the beginning of simulation. In this work, it is considered that the ITZ is the major dissipative zone in the RVE. Also, it is adopted a intrinsic cohesive model (see section 3). These kinds of models and finite elements used here supply accurate responses despite their simplicity, avoiding the need of an adaptive insertion of cohesive elements. Our goal is to model the mechanical behavior of bimodular materials that present recovery of elastic properties due to crack closure using mathematical models simplest as possible by means a computational homogenization-based approach.

Hereafter, it is briefly described the cohesive contact finite element developed in this work. The class of elements considered consists of two surface elements which coincide in space in the undeformed reference configuration of the RVE, Fig. 3. The total number of nodes of the cohesive contact element is 4 (four). The geometry of the finite element is compatible with two-dimensional triangular elements used to model the aggregates and cement paste.

First, consider the local system of the finite element given by ***s*** (sliding direction) and ***n*** (normal direction) coordinate axes. The nodal displacements and internal forces vectors are given by

$$\boldsymbol{u_e} = \begin{Bmatrix} u_e(1) \\ \vdots \\ u_e(4) \\ u_e(5) \\ \vdots \\ u_e(8) \end{Bmatrix} = \begin{Bmatrix} u_e^+ \\ u_e^- \end{Bmatrix} \quad \textit{and} \quad F_e^{\text{int}} = \begin{Bmatrix} F_e^{\text{int}}(1) \\ \vdots \\ F_e^{\text{int}}(4) \\ F_e^{\text{int}}(5) \\ \vdots \\ F_e^{\text{int}}(8) \end{Bmatrix} = \begin{Bmatrix} F_e^{\text{int}+} \\ F_e^{\text{int}-} \end{Bmatrix} \tag{26}$$

The u_e^+ and $F_e^{\text{int}+}$ are the nodal displacements and internal forces vectors related to plus side Γ_e^+. Similarly, the u_e^- and $F_e^{\text{int}-}$ are the nodal displacements and internal forces vectors related to minus side Γ_e^-.

In order to calculate the Gap Function in each Gauss point, the expression below is used

$$\delta_e(\xi_i) = N_e^-(\xi_i(s))u_e^- - N_e^+(\xi_i(s))u_e^+ = u^-(\xi_i) - u^+(\xi_i), i = 1,2,3 \tag{27}$$

Where $u^-(\xi_i)$ and $u^+(\xi_i)$ are the displacements related to Gauss point on minus and plus surface, respectively. $N_e^-(\xi_i(s))$ and $N_e^+(\xi_i(s))$ are shape functions related to Gauss point on minus and plus surface, respectively. Therefore, matrix Ne holds the contribution of shape functions on both sides

$$\boldsymbol{N_e} = \begin{bmatrix} N_e^+ & N_e^- \end{bmatrix} = \begin{bmatrix} N_1(\xi_i) & 0 & N_2(\xi_i) & 0 & N_3(\xi_i) & 0 & N_4(\xi_i) & 0 \\ 0 & N_1(\xi_i) & 0 & N_2(\xi_i) & 0 & N_3(\xi_i) & 0 & N_4(\xi_i) \end{bmatrix} \tag{28}$$

Considering the principle of the virtual work over the crack on plus side Γ_e^+, for example, it can be obtained

$$\delta w_e^{\text{int}+} = \int_{\Gamma_e^+} t(s) \cdot \eta(s) d\Gamma_e = \left[\int_{\Gamma_e^+} N_e^{+T}(s) t(s) d\Gamma_e \right] \begin{Bmatrix} \eta_1^R \\ \eta_1^S \\ \eta_2^R \\ \eta_2^S \end{Bmatrix} \tag{29}$$

The equation above presents the traction internal force vector on the first part and virtual displacements on the second one. Therefore, after some trite calculations, it is possible to obtain the internal force vector at the cohesive contact finite element.

$$F_e^{\text{int}+} = \frac{l_e}{2} \int_{-1}^{+1} N_e^{+T}(\xi) t(S(\xi)) d\xi \tag{30}$$

where l_e is the finite element length and $t(S(\xi))$ is the cohesive traction vector on each Gauss point composed by sliding and normal tractions

$$\boldsymbol{t}(S) = \begin{Bmatrix} t_s(S) \\ t_n(S) \end{Bmatrix} \tag{31}$$

It is important to note that each Gauss point contributes to the calculus of the internal force by means the traction vector obtained by cohesive law (if crack is opened in that Gauss point) or contact law (if crack is closed in that Gauss point). So, in this way, it can get crack surfaces not properly parallel.

For the opened cracks, in loading case, the cohesive traction vector is obtained by means Eqs. (21) and (23) at the Gaus point of interest and its components are given by

$$t_s(\xi_i) = e \frac{\sigma_c}{\delta_c} e^{-\frac{\delta(\xi_i)}{\delta_c}} \beta^2 \delta_s(\xi_i) \tag{32}$$

$$t_n(\xi_i) = e \frac{\sigma_c}{\delta_c} e^{-\frac{\delta(\xi_i)}{\delta_c}} \delta_n(\xi_i) \tag{33}$$

On the other hand, for unloading cases, the cohesive traction vector is obtained by means Eqs. (21) and (24) at the Gaus point of interest and its components are given by

$$t_s(\xi_i) = \frac{t_{\max}(\xi_i)}{\delta_{\max}(\xi_i)} \beta^2 \delta_s(\xi_i) \tag{34}$$

$$t_n(\xi_i) = \frac{t_{\max}(\xi_i)}{\delta_{\max}(\xi_i)} \delta_n(\xi_i) \tag{35}$$

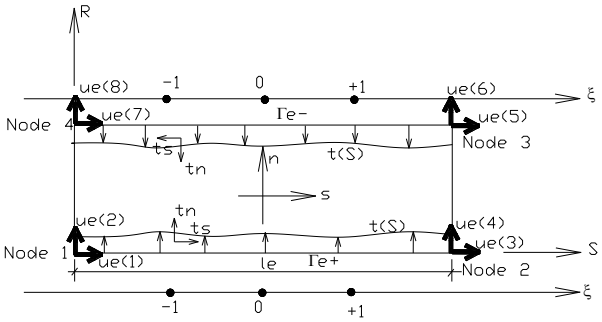

Fig. 3 Geometry of cohesive contact element. The surfaces Γ_e^+ and Γ_e^- coincide in the undeformed reference configuration of the RVE

In the context of implicit finite element computations, $t_{\max}(\xi_i)$ and $\delta_{\max}(\xi_i)$ scalar variables denote the last converged values of the previous increment. However, if the crack surfaces are closed at a Gauss point of interest, the traction vector is denoted by

$$t_s(\xi_i) = \lambda_p l_e \delta_s(\xi_i) \tag{36}$$

$$t_n(\xi_i) = \lambda_p l_e \delta_n(\xi_i) \tag{37}$$

Finally, it should be noted that the integral (Eq. (29)) extends over the undeformed surface of the element in its reference configuration. The integral mentioned may conveniently be approximated by recourse to numerical quadrature using three Gauss points in this work. Then, the internal force vector is given by:

$$F_e^{\text{int}+} \cong \frac{l_e}{2} \sum_{i=1}^{nGauss} N_e^{+T}(\xi_i)\, t(S(\xi_i)) \tag{38}$$

$$F_e^{\text{int}+} = \begin{bmatrix} F_e^{\text{int}+} \\ F_e^{\text{int}-} \end{bmatrix} \tag{39}$$

On the other hand, the internal force vector on the minus side $F_e^{\text{int}-}$ is obtained taking into account that the cohesive traction vector has negative values in order to satisfy the equilibrium of the cohesive contact finite element leading to $F_e^{\text{int}+} = F_e^{\text{int}-}$.

4.1 Consistent linearization: the tangent stiffness matrix

In this work, the linearization of the equilibrium equation system of the RVE for solution of the discrete non-linear boundary value problem is given by

$$R + \frac{dF}{du} d\tilde{u} = 0 \tag{40}$$

where $\boldsymbol{R}$ is the out-of-balance force and $d\tilde{u}$ is the increment of displacement fluctuation field and

calling $\boldsymbol{K}$ the tangent stiffness as $K = \frac{dF}{du}$. Then, focusing on the cohesive contact finite element, the consistent tangent stiffness $\boldsymbol{K_e}$ is written as

$$K_e = \frac{dF_e^{\text{int}}}{du_e} = \begin{bmatrix} \frac{dF_e^{\text{int}+}}{du_e} \\ -\frac{dF_e^{\text{int}-}}{du_e} \end{bmatrix} \tag{41}$$

The component related to minus side needs to take account the direction of cohesive traction vector at that surface. For the plus side, it can observe that

$$\frac{dF_e^{\text{int}+}}{du_e} = \frac{dF_e^{\text{int}+}}{d\delta_e}\frac{d\delta_e}{du_e} \tag{42}$$

$$\frac{dF_e^{\text{int}+}}{d\delta_e} \cong \frac{l_e}{2}\sum_{i=1}^{nGauss} N_e^{+T}(\xi_i)\frac{dt}{d\delta_{eS(\xi_i)}} \tag{43}$$

$$\frac{d\delta_e}{du_e} = \frac{d\left(N_e^-(S)u_e^- - N_e^+(S)u_e^+\right)}{du_e} = = \begin{bmatrix} -N_e^+ & N_e^- \end{bmatrix} = \tag{44}$$

For the minus side, similar equations are obtained. Note that in Eq. (43), it needs to obtain the values of $d\boldsymbol{t}/d\boldsymbol{\delta_e}$ matrix at Gauss point of interest. Therefore, considering an opened crack in loading and unloading cases, the derivate mentioned can be written as, Eqs (45) and (46), respectively

$$\frac{dt}{d\delta_{eS(\xi_i)}} = \begin{bmatrix} \frac{dt_s(\xi_i)}{d\delta_s} & \frac{dt_s(\xi_i)}{d\delta_n} \\ \frac{dt_n(\xi_i)}{d\delta_s} & \frac{dt_n(\xi_i)}{d\delta_n} \end{bmatrix} = \frac{t(\xi_i)}{\delta(\xi_i)} \begin{bmatrix} \beta^2\left[1 - \frac{\beta^2\delta_s^2(\xi_i)}{\delta_c\delta(\xi_i)}\right] & -\frac{\delta_n(\xi_i)\beta^2\delta_s(\xi_i)}{\delta_c\delta(\xi_i)} \\ -\frac{\delta_n(\xi_i)\beta^2\delta_s(\xi_i)}{\delta_c\delta(\xi_i)} & 1 - \frac{\delta_n^2(\xi_i)}{\delta_c\delta(\xi_i)} \end{bmatrix} \tag{45}$$

$$\frac{dt}{d\delta_{eS(\xi_i)}} = \begin{bmatrix} \frac{dt_s(\xi_i)}{d\delta_s} & \frac{dt_s(\xi_i)}{d\delta_n} \\ \frac{dt_n(\xi_i)}{d\delta_s} & \frac{dt_n(\xi_i)}{d\delta_n} \end{bmatrix} = \frac{t_{\max}(\xi_i)}{\delta_{\max}(\xi_i)} \begin{bmatrix} \beta^2 & 0 \\ 0 & 1 \end{bmatrix} \tag{46}$$

However, if the crack surfaces are closed at a given Gauss point of interest, the $d\boldsymbol{t}/d\boldsymbol{\delta_e}$ matrix is expressed by

$$\frac{dt}{d\delta_{eS(\xi_i)}} = \lambda_p l_e \begin{bmatrix} 1 & 0 \\ 0 & 1 \end{bmatrix} \tag{47}$$

5. Numerical applications

The numerical applications of the proposed modeling will be showed in this section. Our main goal here is to show a computational homogenization-based approach as an alternative to complex macroscopic constitutive models for the mechanical behavior of the quasi-brittle materials using a finite element procedure within a purely kinematical multi-scale framework.

This section is composed by numerical examples in order to show the behavior of heterogeneous materials submitted to loading/unloading processes including reversal loads. Besides, it is important to note the behavior of constitutive models implemented in a finite element code to two-dimensional analysis.

It has been cohesive contact finite elements to model the ITZ. Triangle finite elements have been used to model the aggregates and cement paste where the elastic behavior has been adopted. A plane deformation condition is assumed in all analysis. Besides, periodic and linear displacement fluctuations on the boundary of the RVEs are assumed.

5.1 Validation of the constitutive model

This numerical application deals with a RVE with a single cohesive contact finite element located at the centre. A periodic condition is imposed on the boundary of the RVE. It intends to verify the behavior of the contact model as well as the cohesive law when this RVE is submitted to loading/unloading process including reversal load.

The RVE is illustrated in Fig. 4. The parameters of the cohesive and contact models are given in Table 1 as well as the Young's modulus E and Poisson's ratio ν. The symmetric mesh of triangle finite elements is very poor (14 elements), but the focus here is the behavior of the cohesive contact finite element.

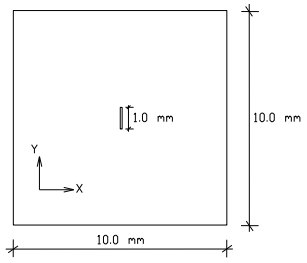

Fig. 4 Geometry of the RVE with a single cohesive contact finite element

Table 1 Elastic, cohesive fracture and contact model parameters

E (N/mm^2)	ν(-)	δ_C (mm)	σ_C (N/mm^2)	β (-)	λ_p (N/mm)
30000	0.2	0.0002	4	0.707	10^7

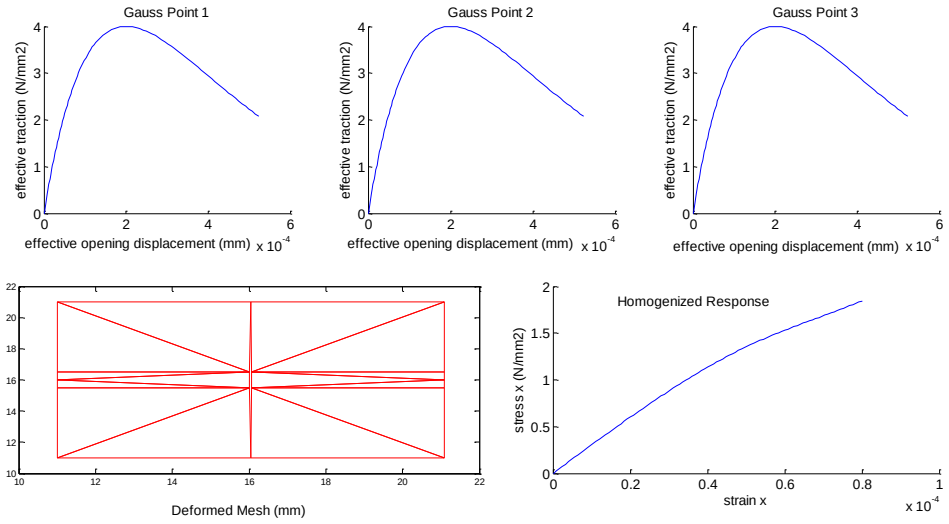

Fig. 5 Behavior of the cohesive fracture model on the RVE - loading case 1

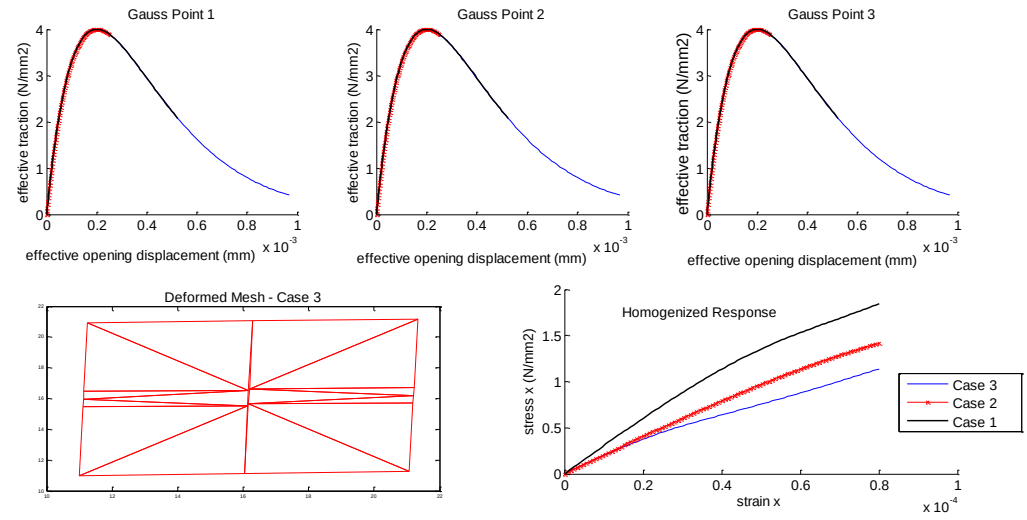

Fig. 6 Behavior of the cohesive fracture model on the RVE - loading cases 1, *2* and 3

Initially, the behavior of the cohesive model has been analyzed. Regarding the Cartesian axes illustrated in Fig. 4 and followed throughout the paper, we have applied a total strain $\boldsymbol{\varepsilon} = [0.00008; 0; 0]$ in 20 increments and we have called loading case 1, where $\boldsymbol{\varepsilon} = [\varepsilon_x; \varepsilon_y; \gamma_{xy}]$ and it was used

10^{-7} as tolerance value. It is observed in Fig. 3 the perfect behavior of the cohesive fracture model in each Gauss point (see the three graphs in top) by means the three similar graphs t_{ef} (N/mm^2) x δ_{ef} (mm). In the bottom of Fig. 5, it can be observed the mesh adopted and the cohesive contact finite element opened (there is a deformation amplification factor used only for plotting the deformed micro-cell mesh). Also, it can observe the graph of homogenized response about σ_x (N/mm^2) x ε_x. It can be noted the influence of the fracture process in the homogenized response of the RVE.

Also, we have submitted RVE to the loading cases *2* and *3*, where $\boldsymbol{\varepsilon}$ = [0.00008; -0.00008; 0] and $\boldsymbol{\varepsilon}$ = [0.00008;-0.00008; 0.0005], respectively. The Fig. 6 shows the deformed mesh to case 3 and the homogenized responses plotted in the same graph in order to compare them. It is noted the behavior more damaged of the RVE when the loading conditions are increased.

Another interesting observation can be verified about the Fig. 7, where there are some graphs representing the loading case 1 and the increasing of the maximum cohesive normal traction, σ_C. In Fig. 7, Case 1 refers to σ_C = 4 N/mm^2, Case 2 refers to σ_C = 40 N/mm^2 and Case 3 refers to σ_C = 0.4 N/mm^2. The behavior of the RVE seems like an elastic RVE (without fracture) when the σ_C has been increased. On the other hand, when σ_C has been decreased, the RVE starts to present a behavior like a medium with a strong fracture without a transition process. These results show coherent qualitative numerical responses of the cohesive model implemented in a finite element procedure within a purely kinematical multi-scale framework.

Finally, the RVE is submitted to a loading/unloading including reversal loading. Now, it intends to verify the behavior of cohesive and contact model in conjunction with cohesive contact finite element developed in this work. In the first case, we have applied a loading with total strain $\boldsymbol{\varepsilon}$ = [0.00008; -0.00008; 0.0005], then we have proceeded to complete unloading up to reversal loading in compression up to $\boldsymbol{\varepsilon}$ = [-0.00004; -0.00004; -0.00025]. As it can see in Fig. 8, the cohesive contact finite element is closed and the unilateral effect in this simple example is perfectly modeled. The transition between cohesive and contact law seems quite satisfactory to model that phenomenon. Once more, the qualitative responses are quite satisfactory.

5.2 Validation of the modeling proposal for heterogeneous material

Now, the proposed modeling is applied to simulate the mechanical behavior of a heterogeneous material with inclusions disposed into the RVE following a uniformly random distribution proposed by Nguyen *et al.* (2011).

For these numerical examples, a plane stress conditions is adopted. The parameters of the contact and cohesive models are given in Table 2.

Table 2 Elastic parameters and parameters of the cohesive and contact models

	E (N/mm^2)	ν(-)	δ_C (mm)	σ_C (N/mm^2)	β (-)	λ_p (N/mm)
ITZ			0.0002	4	0.707	10^5
Aggregate	30000	0.2				
Matrix	25000	0.2				

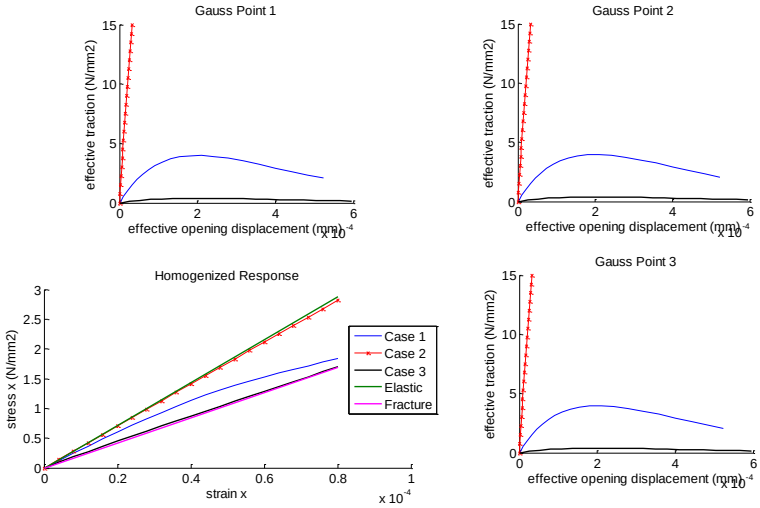

Fig. 7 Study about the behavior of the RVE- loadings with different σ_c

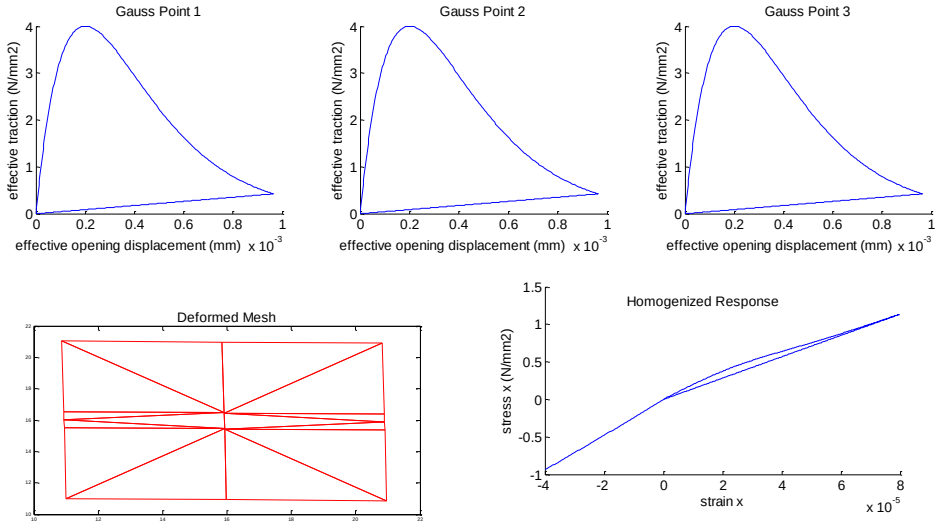

Fig. 8 Loading/unloading case - unilateral behavior of the RVE

5.2.1 Elastic-fracture behavior

This numerical example intends to show the behavior of the proposed modeling in this work when applied to a RVE of a heterogeneous material like concrete, for example. Sizes of aggregates are varied from 2.5 mm to 5.0 mm. The RVE has dimensions 10 x 10 mm with 45% of inclusions, see Fig. 9. A periodic condition is imposed on the boundary of the RVE. Here, it intends to verify the behavior of the ITZ during the loading process.

The mesh is composed by 520 triangle elements where 187 elements are used to model the aggregates and 333 elements are used to model the cement paste (matrix). Besides, 95 cohesive contact finite elements are used to model the ITZ in all surroundings of aggregates.

Initially, it has been applied a total strain $\boldsymbol{\varepsilon} = [0.00022; 0; 0]$ (case1) in 20 increments using a tolerance of 10^{-6}. It is observed in Fig. 10 the homogenized response about σ_x (N/mm^2) x ε_x. It can be noted that the non-linearity of the response is linked to the increase of the number of cracks in the ITZ. The cohesive model adopted in this work assumes that in the beginning of the deformation process there is a fracture created. However, its effective opening is linked to how is growing the applied load. This is reasonable when we are dealing with deformation processes at microstructure level. Nevertheless, the homogenized response σ_x x ε_x starts to present some energy dissipation when there is a increasing of the number of cracks. Therefore, a junction of some cracks in the ITZ leads to a non-linearity of the homogenized response more pronounced. This phenomenon can be seen in Fig. 10 by means a close-up view in the ITZ corresponding to $\sigma_x = 4.8$ N/mm^2.

Paulino *et al.* (2008) have mentioned convergence problems in simulations that use intrinsic cohesive models. In fact, when the number of activated cohesive elements is increased, mainly at the peak of the σ x ε curve when there are many cracks at the ITZ, the iterative process presents a increasing of iterations. However, the consistent tangent formulation adopted in this work (see section 4.1) shows a robustness and efficient numerical solution. This is very important when dealing with multi-scale analysis and this is the authors' goal in future works.

Also, the RVE has been submitted to total strain $\boldsymbol{\varepsilon} = [0; 0.00022; 0]$ (case 2) in order to verify the anisotropic behavior of the material. Fig. 11 shows the comparison between the numerical responses when the RVE is loaded in the x-direction and y-direction. It is observed that the difference between the responses arises at peak stress region of the homogenized stress-strain relation. In fact, this anisotropic behavior takes place when there is a union of microcracks in the ITZ surrounding the aggregates. Also, note the differences between the microcrack configurations, see Fig.12 that shows a close-up view at the large aggregate. Therefore, the proposed modeling is capable to simulate the anisotropic behavior of the heterogeneous materials due to geometry and the distribution of aggregates on the RVE.

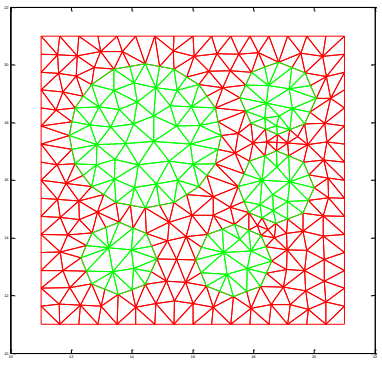

Fig. 9 Mesh of the RVE

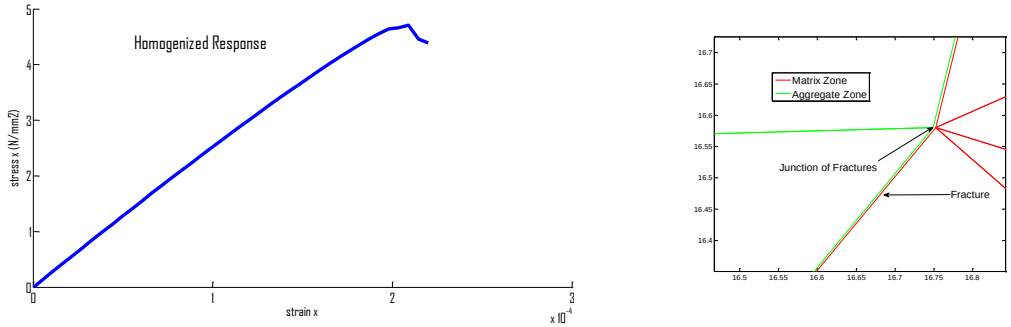

(a) homogenized response (b) close-up view of the ITZ

Fig. 10 RVE of a heterogeneous material

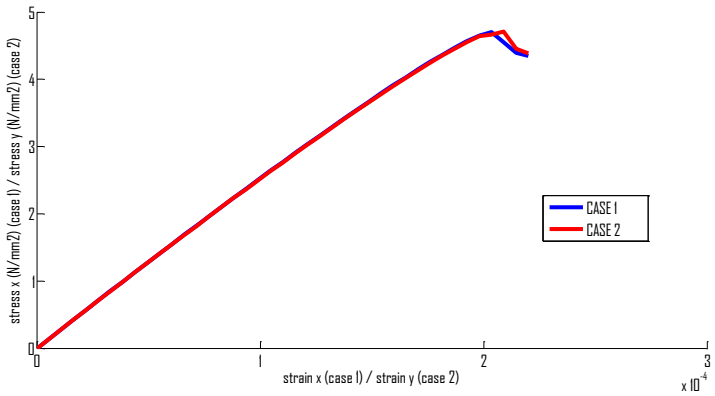

Fig. 11 Anisotropic behavior of the RVE - homogenized response

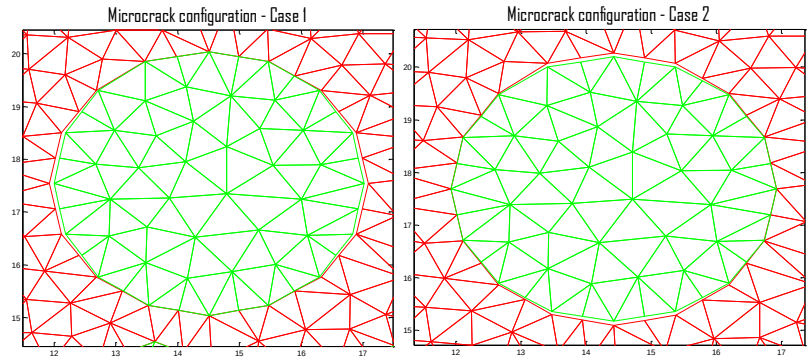

Fig. 12 Anisotropic behavior of the RVE - microcrack configurations

In order to check the objectivity of the numerical responses, a mesh with 8088 triangle finite elements and 364 cohesive contact finite elements was used. A linear condition has been imposed on the boundary of the RVE. As it can see in Fig. 13, the numerical responses did not change. The new mesh is plotted in the same figure with a deformation amplification factor in order to visualize the microcracks opened.

Now, it intends to investigate the influence of the shape of aggregates in the homogenized stress-strain relation. For this reason, the original circular aggregates have been replaced by ellipsoid aggregates trying to agree the center of the two shapes. Fig. 14 shows the new RVE. A mesh with 851 triangle finite elements and 94 cohesive contact finite elements was used.

In this analysis, it has been applied a total strain $\boldsymbol{\varepsilon} = [0.0003; 0; 0]$ in 20 increments using a tolerance of 10^{-6}. The homogenized response is plotted in the Fig. 15. Also, it is possible to compare the numerical responses of the RVEs with circular and ellipsoid aggregates. Note that, for this numerical example, the homogenized response seems more flexible for ellipsoid shape than for circular shape evidencing once more time the importance of the geometry of the material components on the mechanical behavior of the RVE. Obviously, it is necessary to perform a significant number of analyses, but we have not considered many different samples since a statistical analysis of the existence of an RVE for this kind of material has already been given in Nguyen *et al.* (2010).

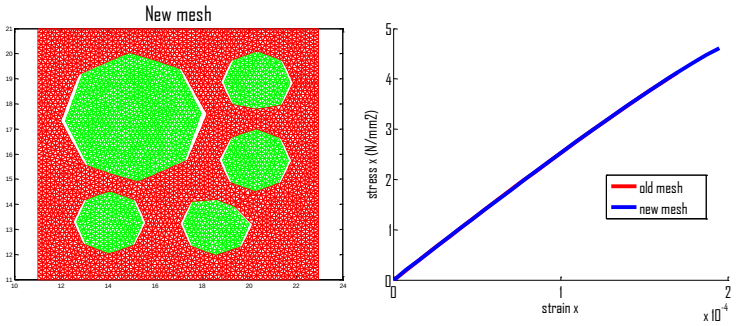

Fig. 13 Numerical responses of the old and new meshes

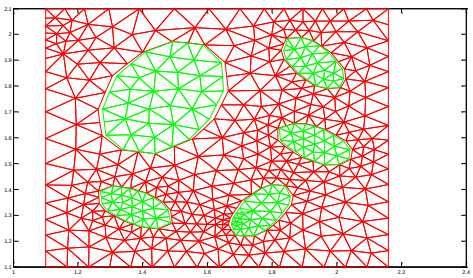

Fig. 14 Mesh of the RVE with ellipsoid aggregates

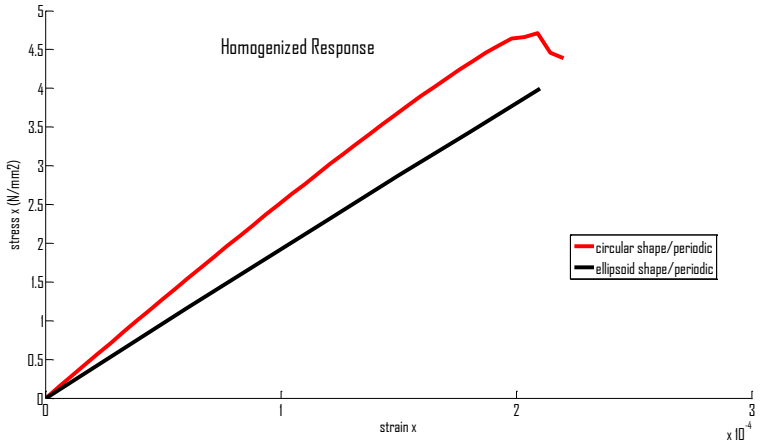

Fig. 15 Numerical responses of the RVE with circular and ellipsoid aggregates

5.2.2 Unilateral effect

This numerical example intends to show the potentialities of the proposed modeling in this work related to capture of the unilateral effect of the RVE of a heterogeneous material like concrete, for example. The same RVE and finite element mesh of the last numerical example are used here, see Fig. 9.

Initially, periodic and linear conditions are imposed on the boundary of the RVE in order to verify the stiffest and more compliant solution of the microscopic equilibrium problem.

The RVE is submitted to a loading/unloading including reversal loading. Now, it intends to verify the bimodular behavior of the RVE of a brittle material. We have applied a loading with total strain $\boldsymbol{\varepsilon}$ = [0.00023; 0; 0.], then we have proceeded to complete unloading up to reversal loading in compression up to $\boldsymbol{\varepsilon}$ = [-0.00045; 0.; 0.]. A total of 60 increments have been performed and a tolerance of 10^{-6} has been used.

As it can see in Fig. 16, the unilateral effect in brittle material analyzed here is perfectly modeled. The transition between cohesive and contact law seems quite satisfactory to model that phenomenon. Once more, the qualitative responses are quite satisfactory, like as in section 5.1. Note that, initially, the numerical responses are very similar, but when the dissipation processes take place, like fracture and contact problems, a difference between the periodic and linear conditions is more evident. The linear condition gives the stiffest solution. These conclusions are agreement with Peric *et al.* (2011). Nevertheless, the proposed modeling is not capable to capture the dissipation processes quite satisfactory in compression stress regimes, despite the opened microcracks due to Poisson effect.

Now, it has been adopted different values for the penalty factor (λ_p), see section 3.2. It intends to investigate the influence of this parameter in the recovery of material stiffness when the RVE is submitted to reversal loading.

For Ju *et al.* (1995), a very large penalty factor leads to accurate numerical solution as well as to convergence problems. Otherwise, a small penalty factor usually results in easy convergence, but the numerical results might be less reliable. Therefore, there is a dependency upon the choice of penalty factor in order to obtain a reliable result.

For this analysis, the values for penalty factor from 10^4 up to 10^9 N/mm have been adopted. This technique is similar to used by Ju *et al.* (1995). Note that, for high values, the penalty factor does not influence the behavior of the numerical responses, see Fig. 17. Besides, during the analyses it has been observed a increasing of the number of iterations in order to close the microcracks for high values of penalty factor. In this numerical example, the value 10^7 can be considered as a reasonable penalty factor which not only produces convergence but would give reliable results, see Fig. 17.

In general, the robustness of the Newton–Raphson scheme adopted in the iterative solution of the incremental RVE equilibrium problem has been evidenced in all numerical applications. A quadratic rate of asymptotic convergence of the microscopic scale Newton–Raphson scheme has been achieved. The problems have presented up to four iterations to obtain an accurate response even dealing with contact problems. This feature is important when dealing with multi-scale analyses.

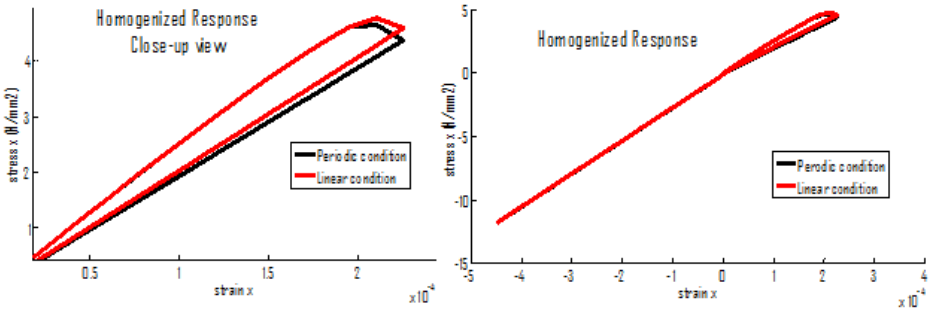

Fig. 16 Numerical responses of the RVE: close-up and global views

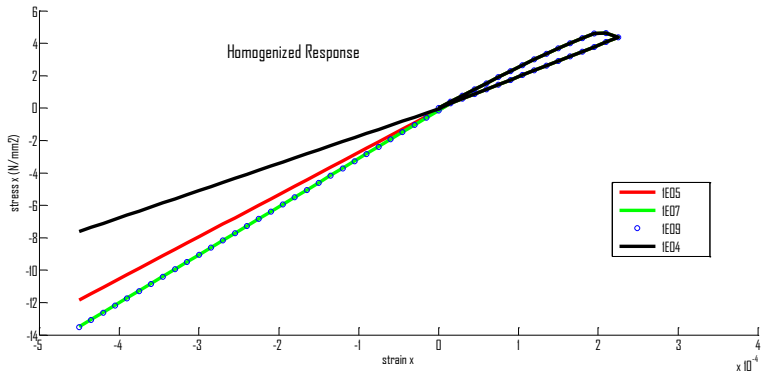

Fig. 17 Influence of the penalty factor on the numerical response

6. Conclusions

In this work, numerical applications of a computational homogenization-based approach proposed to model the mechanical behavior of heterogeneous materials subject to reversal loading have been presented.

A cohesive contact finite element has been developed in order to take into account opening and closing processes. This finite element has been implemented in a 2D finite element code to analyze RVEs within a purely kinematical multi-scale framework developed by Péric *et al.* (2010) and Giusti *et al.* (2009).

The qualitative responses presented are quite satisfactory considering that only simple cohesive and contact models were employed. Besides, it is important the results obtained here about the modeling of unilateral effect in brittle materials. Also, the model is able to obtain homogenized responses of bimodular materials (different behaviors in tension and compression regimes) and anisotropy induced by damage processes. These results show that the modeling developed in this work is potentially applicable in multi-scale analysis of concrete structures submitted to cyclic loading.

In general, the numerical responses have been obtained an easy convergence even when contact problems arise due to closed microcracks. The self-consistent linearization developed here has presented a computational efficiency which is expected to be particularly useful for multi-scale analysis of heterogeneous materials.

Therefore, these initial results encourage us to procedure in the improvement of the modeling proposed in this work in order to use it in the parametric identification of complex macroscopic constitutive models and multi-scale analysis of concrete structures. It can be incorporated the Mohr-Coulomb model in order to contribute to the dissipated energy in the cement paste zone and to simulate the plastic strains together with cohesive and contact models, for example. As a reminder, we are trying to model a complex macroscopic behavior using simplest as possible as constitutive models at mesoscopic scale. The features discussed here will be addressed in future works.

Acknowledgements

The financial support from CAPES Foundation, Ministry of Education of Brazil (Grant n. BEX 0805/11-4) is gratefully acknowledged.

References

Brancherie, D. and Ibrahimbegovic, A. (2009), "Novel anisotrtopic continuum-discrete damage model capable of representing localized failure of massive structures. Part I: theoretical formulation and numerical implementation", *Eng. Comput.*, **26**(1-2), 100-127.

Carol, I., López, C.M. and Roa, O. (2001), "Micromechanical analysis of quasi-brittle materials using fracture-based interface elements", *Int. J. Numer. Meth. Eng.*, **52**(1-2), 193-215.

Cirak, F., Ortiz, M. and Pandolfi, A. (2005), "A cohesive approach to thin-shell fracture and fragmentation", *Comput. Method. Appl. M.*, **194**(21-24), 2604-2618.

Gal, E. and Kryvoruk, R. (2011), "Fiber reinforced concrete properties – a multiscale approach", *Comput. Concr.*, **8** (5), 525-539.

Giusti, S.M., Blanco, P.J., de Souza Neto, E.A. and Feijóo, R.A. (2009), "An assessment of the Gurson yield criterion by a computational multi-scale approach", *Eng. Computation*, **26**(3), 281-301.

He, H., Stroeven, P., Stroeven, M. and Sluys, L.J. (2011), "Influence of particle packing on fracture properties of concrete", *Comput. Concr.*, **8** (6), 677-692.

Ju, S. H., Stone, J.J. and Rowlands, R.E. (1995), "A new symmetric contact lement stiffness matrix for frictional contact problems", *Comput. Struct.*, **54** (2), 289-301.

Michel, J.C., Moulinec, H. and Suquet, P. (1999), "Effective properties of composite materials with periodic microstructure: a computational approach", *Comput. Method. Appl. M.*, **172**(1-4)**,** 109-143

Miehe, C., Schröder, J. and Schotte, J., (1999), "Computational homogenization analysis in finite plasticity simulation of texture development in polycrystalline materials", *Comput. Method. Appl. M.*, **171**(3-4), 387-418.

Nguyen, V.P., Lloberas Valls, O., Stroeven, M. and Sluys, L.J. (2010), "On the existence of representative volumes for softening quasi-brittle materials – a failure zone averaging scheme", *Comput. Method. Appl. M.*, **199** (45-48), 3026-3036.

Nguyen, V.P., Lloberas Valls, O., Stroeven, M. and Sluys, L.J. (2011), "Homogenization-based multiscale crack modelling: from micro-diffusive damage to macro-cracks", *Comput. Method. Appl. M.*, **200** (9-12), 1220-1236.

Ortiz, M. and Pandolfi, A. (1999), "Finite-deformation irreversible cohesive elements for three-dimensional crack-propagation analysis", *Int. J. Numer. Meth. Eng.*, **44**(9), 1267-1282.

Paulino, G.H., Celes, W., Espinha, R. and Zhang, Z. (2008), "A general topology-based framework for adaptative isertion of cohesive elements in finite element meshes", *Eng. Computation*, **24**(1), 59-78.

Peric, D., de Souza Neto, E.A., Feijóo, R.A., Partovi, M. and Carneiro Molina, A.J. (2011), "On micro-to-macro transitions for multiscale analysis of heterogeneous materials: unified variational basis and finite element Implementation", *Int. J. Numer. Meth. Eng.*, **87**(1-5), 149-170.

Pituba, J.J.C. and Fernandes, G.R. (2011), "An anisotropic damage model for concrete", *J. Eng. Mech-ASCE.*, **137**(9), 610-624. DOI: 10.1061/(ASCE)EM.1943-7889.0000260.

Somer, D.D., de Souza Neto, E.A., Dettmer, W.G. and Peric, D. (2009),. "A sub-stepping scheme for multi-scale analysis of solids", *Comput. Method. Appl. M.*, **198**(9-12), 1006-1016.

Terada, K., Saiki, I., Matsui. K. and Yamakawa, Y. (2003), "Two-scale kinematics and linearization for simultaneous two-scale analysis of periodic heterogeneous solids at finite strains", *Comput. Method. Appl. M.*, **192**(31-32), 3531- 3563.

Unger, J.F. and Eckardt, S. (2011a), "Multiscale modeling of concrete", *Arch. Comput. Method. E.*, **18**(3), 341-393.

Unger, J.F., Eckardt, S. and Könke, C. (2011b), "A mesoscale model for concrete to simulate mechanical failure", *Comput. Concr.*, **8**(4), 401-423.

Verhoosel, C.V., Remmers, J.J.C., Gutiérrez, M.A. and de Borst, R. (2010), "Computational homogenisation for adhesive and cohesive failure in quasi-brittle solids", *Int. J. Numer. Meth. Eng.*, **83** (8-9), 1155-1179.

Wriggers, P. and Reinelt, J. (2009), "Multi-scale approach for frictional contact of elastomers on rough rigid surfaces", *Comput. Method. Appl. M.*, **198**(21-26), 1996-2008.

Wriggers, P. (2006), *Computational contact mechanics*, Springer-Verlag, Berlin.

Xiaoyu, J., Jianping, Q., Chenghua, W. and Yu, Z. (2006), "Computer simulation of landslides by the contact element method", *Comput. Geosci-UK*, **32**(4), 434-441.

Zhu, Q., Kondo, D., Shao, J. and Pensee, V. (2008), "Micromechanical modelling of anisotropic damage in brittle rocks and application", *Int. J. Rock Mech. Min.*, **45**(4), 467-477.

Zhu, Q., Kondo, D. and Shao, J. (2009), "Homogenization-based analysis of anisotropic damage in brittle materials with unilateral effect and interactions between microcracks", *Int. J. Numer. Anal. Met.*, **33**(6), 749-772.

List of Symbols

$\boldsymbol{\varepsilon}$	Macro strain tensor
$\boldsymbol{\varepsilon}_\mu$	Micro strain tensor
$\mathbf{D}^{\text{hom}}$	Homogenized fourth order constitutive tensor
$\boldsymbol{D}^{\text{Taylor}}$	Fourth order constitutive tensor for Taylor boundary conditions
$\widetilde{\boldsymbol{D}}$	Fourth order constitutive fluctuation tensor
$\mathbf{n}$	Outward unit normal field
$\boldsymbol{q}$	Internal variables vector
$\boldsymbol{t}$	Cohesive traction vector over the crack
t	Scalar effective traction
$\mathbf{u}_\mu$	Microscopic displacement field
$\widetilde{\boldsymbol{u}}_\mu$	Displacement fluctuation field
V_μ	Volume of the RVE
x	Point of the continuum media
y	Point of the microstructure
β	Parameter that defines the ratio between the shear and the normal critical tractions
$\boldsymbol{\delta}_s$	Sliding opening displacements
$\boldsymbol{\delta}_n$	Normal opening displacements
δ_c	Characteristic opening displacement